https://doi.org/10.5194/egusphere-2025-3091
Preprint. Discussion started: 9 September 2025

Drought-induced land use and land cover change impacts on hydrology: Insights from the Harz mountains, Germany

Paul D. Wagner[1,2*], Fatemeh Saba[3], Pedro Achanccaray[3] and Nicola Fohrer[2]

[1]Applied Physical Geography -Environmental Hydrology and Resource Management, Department of Earth Sciences, Freie Universität Berlin, D-12249 Berlin, Germany (*paul.wagner@fu-berlin.de)
[2]Department of Hydrology and Water Resources Management, Kiel University, D-24118 Kiel, Germany
[3]Institute of Geodesy and Photogrammetry, Technische Universität Braunschweig, D-38106 Braunschweig, Germany

Correspondence to: Paul D. Wagner (paul.wagner@fu-berlin.de)

https://doi.org/10.5194/egusphere-2025-3091
Preprint. Discussion started: 9 September 2025

Abstract:

Drought conditions in Europe in 2018 and the following years led to significant land use and land cover (LULC) changes that affect the water balance. One of the regions that experienced strong changes are the Harz mountains in Germany, where drought conditions have led to tree mortality in its forested catchment areas. The aim of this study is to quantify these drought-induced LULC changes and analyze how they affect the water and sediment balance. To this end, remote sensing data and a deep learning model were used to derive annual LULC changes including dead tree areas between 2018 and 2023. These data were used to set up a SWAT+ model with dynamic LULC changes. The model was calibrated at the gauges of three headwater catchments of the Oker river. Kling-Gupta efficiencies indicate varying but at least satisfactory performance at all gauges during calibration (0.75 to 0.82) and validation period (0.63 to 0.79). Areas of dead trees were modeled as bare or sparsely vegetated (recent tree mortality) or as grassland (regrown areas). The LULC change analysis demonstrated strong performance (86–88% overall accuracy) and revealed a decrease in coniferous trees by up to 46% in one catchment (19% and 25% in the others). The hydrologic impacts were assessed by comparing a model run with LULC changes to a run without LULC changes. The results indicate a continuous decrease of evapotranspiration by up to -7.4% in 2023 and a continuous increase of water yield by up to 11.3% in 2023. The spatial assessment of modeled LULC change impacts shows strong increases in water yield and percolation and strong decreases in evapotranspiration associated with tree mortality. The increase in water yield can mainly be attributed to an increase in surface runoff. Changes in sediment yield indicate increased risk of soil erosion at areas associated with tree mortality. It was found that a dynamic model representation of tree mortality is necessary to account for these fast and strong changes and their impacts on hydrology. Moreover, the faster response of the catchment potentially increases the severity of flood events and the flood risk in downstream areas. The results underline that droughts significantly affect hydrology even after the end of the drought event. Therefore, afforestation with climate-resilient trees is needed to improve both flood and drought resilience in regions that suffer from drought-induced tree mortality.

Keywords: *Land use and land cover change, SWAT+, hydrologic extremes, Harz mountains*

https://doi.org/10.5194/egusphere-2025-3091
Preprint. Discussion started: 9 September 2025

1. Introduction

Europe has suffered from extreme drought conditions in 2018 and the following years. Rakovec et al. (2022) underline that the 2018-2020 drought event had an unprecedented intensity. Moreover, the drought in 2022 was among the most extreme ones with regard to soil moisture within the last 60 years (Bevacqua et al. 2024). While the recent drought conditions had obvious direct impacts on the water balance during the prevailing drought, indirect effects affect the water balance after the event. One of these indirect impacts are drought-induced land use and land cover (LULC) changes like the loss of vegetation that affect the water balance. LULC changes affect droughts and floods and Auerswald et al. (2025) argue that this driver is even more important than increasing temperatures.

Forests are an important carbon sink and therefore essential for climate protection. However, forests are also affected by climate change and forest loss exacerbates climate change. In the Mediterranean Basin forest regression and dieback can be observed due to increasing drought conditions (Peñuelas & Sardans, 2021). However, these developments can now also be observed in temperate climates: The Harz mountains in central Germany have experienced strong LULC changes in the last decade. The prevailing coniferous (spruce) trees are drought sensitive (Sutmöller & Meesenburg, 2018). Therefore, during the drought event these trees became more vulnerable to bark beetle resulting in large areas of dead trees. These areas exponentially increased between 2015 and 2020 in the Harz mountains (Kong et al. 2022).

In general, tree mortality results in an increase of runoff and a decrease of evapotranspiration, although impacts can differ considerably, depending on catchment characteristics (Adams et al. 2012, Zhang et al. 2017). In a global synthesis, Hou et al. (2023) found that hydrological sensitivity to changes in forest cover is higher in catchments with a large percentage of the same tree species and little water retention capacity. These are characteristics that can also be found in low mountain ranges like the Harz mountains, underlining the exposure of the study area to potentially strong impacts.

To adequately assess the impacts of such exponential changes, models are required that allow for a dynamic representation of LULC changes (Wagner et al. 2019). Using the cases of three headwater catchments in the Harz mountains, we aim at i) assessing annual drought-induced LULC changes between 2018 and 2023, ii) representing these dynamic LULC changes in a hydrologic model, and iii) assessing the temporal and spatial impacts of continuous LULC changes on water balance components.

2. Methodology

2.1 Study area

The study area is composed of three headwater catchments belonging to the Oker river catchment in the Harz mountains, Germany (Figure 1). The three catchments are defined by the gauges Sennhütte at river Gose (6.1 km²), Altenau (I) at river Oker (31.6 km²), and Bad Harzburg (I & II) at river Radau (18.1 km²). In total, they cover an area of 55.8 km². The elevation ranges from 360 m to 763 m in the Gose catchment, 407 m to 821 m in the Radau catchment, and 418 m to 929 m in the

https://doi.org/10.5194/egusphere-2025-3091
Preprint. Discussion started: 9 September 2025

Oker catchment. LULC is characterized by the predominance of coniferous forest. However, following drought conditions in 2018, a large percentage of coniferous trees died.

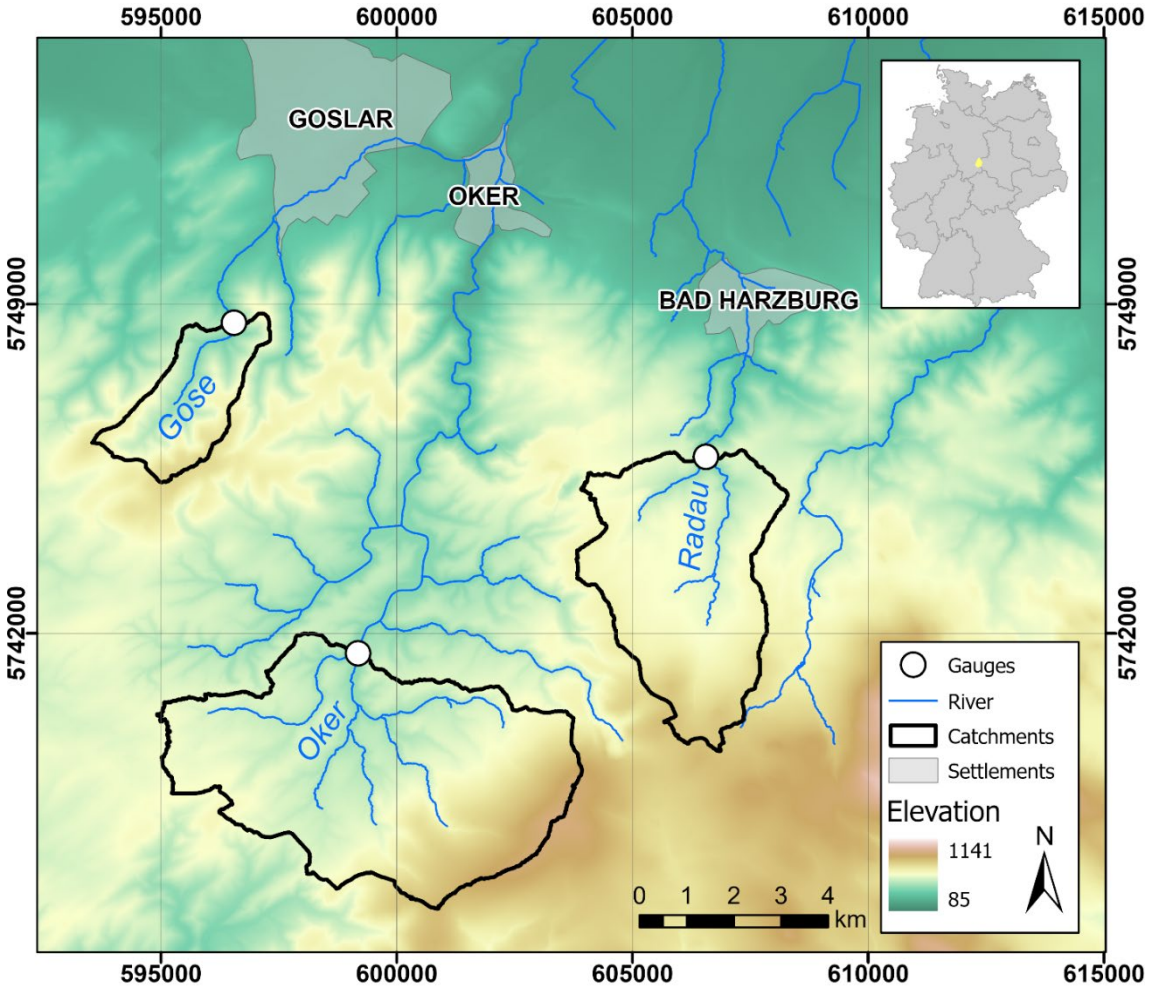

Figure 1: The three headwater catchments in the Harz mountains with stream network, gauges, major settlements and topography, based on elevation data from LGLN (2022).

2.2 Land use and land cover classifications

Annual LULC classifications between 2018 and 2023 were prepared based on multi-temporal multi-sensor satellite data. For the classification, optical Sentinel-2 and radar Sentinel-1 data from the growing season (June-August) were used. The Sentinel-2 Level-2A images with 10 spectral bands in the visible, the red-edge, the NIR regions and the shortwave infrared regions, various spatial resolutions (10, 20 m) and cloud cover lower than 5% were acquired. The 20 m bands were

https://doi.org/10.5194/egusphere-2025-3091
Preprint. Discussion started: 9 September 2025

resampled to 10 m, and a cloud mask was applied to the Sentinel-2 data. For Sentinel-1 images, dual-polarization C-band Ground Range Detected dataset with a spatial resolution of 10 m was applied. Ground truth data included ESA WorldCover maps for 2020 and 2021 for land cover types (ESA WorldCover 2020, 2021), a European LULC map -ELC10- (Venter & Sydenham, 2021), a tree species map for classifying coniferous and deciduous trees (Blickensdörfer et al., 2024) and manually collected samples of dead trees derived from high-resolution Planetscope images (https://www.planet.com/explorer). The ground truth data were split randomly into training, validation, and test dataset at a ratio of 70:10:20, respectively. The training and validation datasets were used during the training process, while the test dataset was used to evaluate the model's performance.

As classification algorithm U-Net (Ronneberger et al., 2015), a well-known convolutional neural network (CNN) that comprises an encoder, bottleneck, and decoder was applied. To this end, the input data was represented as a 3-dimensional tensor (256 × 256 × 19), where 256 × 256 represents the width and height of the patch and 19 represents the number of channels. These channels included 10 spectral bands and 7 vegetation indices generated from Sentinel-2 (SAVI, NDVI, NDVI_rededge, IBI, MNDWI, GNDVI, NDBI) (Appendix, Table A1), along with two polarizations (VV and VH) from Sentinel-1 images.

In the encoder, the input images passed through three convolutional blocks, each with two convolutional layers (64, 128, and 256 filters of size 3×3), followed by batch normalization and ReLU activation. Furthermore, a max-pooling layer was employed to downscale the spatial resolution to 2×2 matrices, thereby enhancing spectral resolution. Subsequently, in the decoder, additional convolutional blocks, including transpose convolutions were utilized to reverse the encoder's effects, thereby restoring spatial resolution for LULC classification. The model used multi-class cross-entropy as the loss function and Adam as the optimizer, generating a 7-dimensional array that assigned pixel probabilities to the target classes. Overall, the following seven LULC classes were considered: cropland, grassland, built-up areas, water body, coniferous, deciduous, and dead trees.

In addition, data augmentation techniques such as rotation and flipping were applied during training to enhance the model's generalization and robustness. Moreover, U-Net trained up to 100 epochs with an early stopping, to avoid overfitting, of 10 epochs without improvement in the validation loss value.

To evaluate the model's performance, overall accuracy, F1-score, recall and precision derived from confusion matrix were calculated as follows:

$$Overall\ accuracy = \frac{TP+TN}{TP+TN+FP+FN} \quad (1)$$

$$F1_{score} = \frac{Presicion \times Recall}{Presicion+Recall} \times 2 \quad (2)$$

$$Precision = \frac{TP}{\mathrm{TP+FP}} \quad (3)$$

$$Recall = \frac{TP}{\mathrm{TP+FN}} \quad (4)$$

https://doi.org/10.5194/egusphere-2025-3091
Preprint. Discussion started: 9 September 2025

Where TP (True Positive) represents the number of correctly classified pixels belonging to the target class, TN (True Negative) is the number of correctly classified pixels that do not belong to the target class. FP (False Positive) is the number of pixels incorrectly classified as belonging to the target class, and FN (False Negative) is the number of pixels of the target class that were incorrectly classified as not belonging to it.

The applied workflow for LULC classification is presented in Figure 2: The 2D U-Net model was trained using satellite images and ground truth data from 2020 and 2021. Following training, the model's performance was evaluated using test data from these years as well as from 2018. To generate annual LULC maps, the trained model was subsequently applied to data from other years. Each image for each year was processed individually through the model, and the predictions were combined using majority voting approach to produce the final annual LULC map.

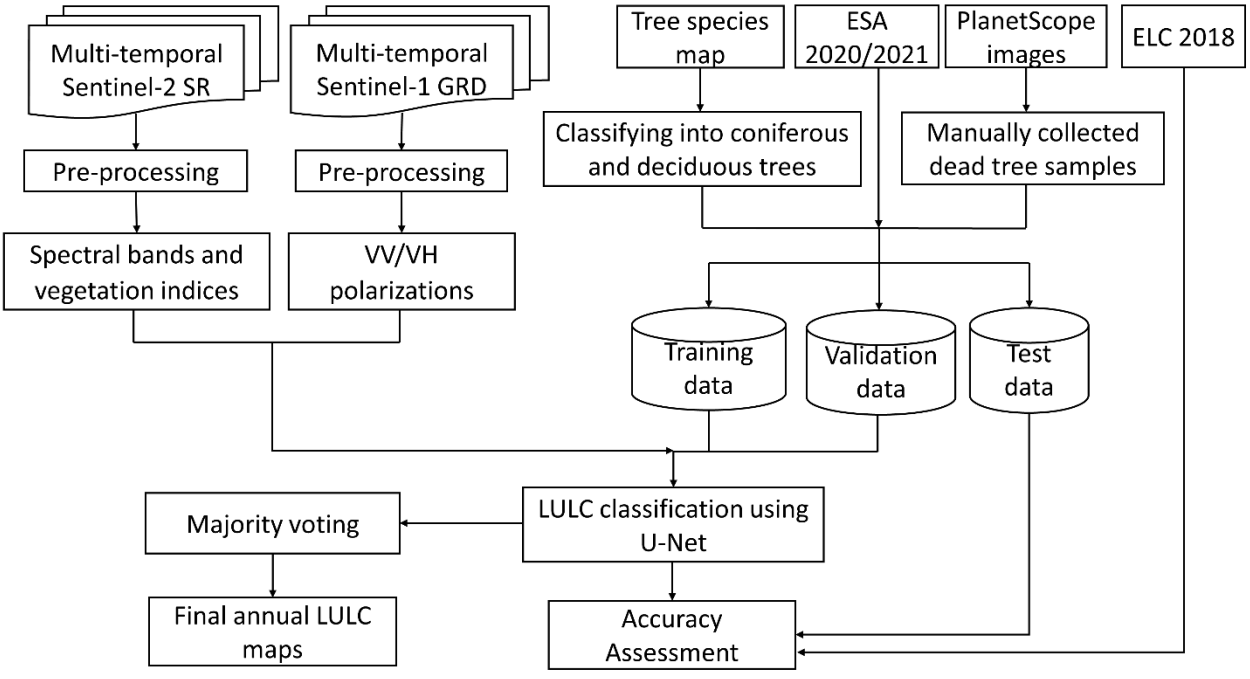

Figure 2: Applied workflow for LULC classification.

2.3 Hydrologic model

The latest version of the Soil and Water Assessment Tool (Arnold et al. 1998), SWAT+ (Bieger et al. 2017, revision 61.0.1) was used to model the water balance and assess the impact of dynamic LULC changes on water balance components. SWAT+ is a semi-distributed catchment model that uses hydrologic response units (HRUs) defined by the same LULC, soil, and slope class in a sub-catchment, as smallest computational unit.

https://doi.org/10.5194/egusphere-2025-3091
Preprint. Discussion started: 9 September 2025

To derive the HRUs we used i) a digital elevation model with a spatial resolution of 5 meters (upscaled from DEM1, LGLN 2022) to derive five slope classes using thresholds at 2%, 9%, 15%, and 25%, ii) a soil map with a spatial resolution of 1:200 000 (BGR 2022) refined for peat soil areas with the information from a 1:50 000 (LBEG 2024) that was parameterized for SWAT+, and iii) annual LULC classifications with a spatial resolution of 10 m (2.2) parameterized with suitable LULC classes from the SWAT plant database. We used the temperate mountain forest parameterization for coniferous forest (frse_tems), deciduous forest (frsd_tems), and grassland (rnge_tems). Settlement areas were modelled with an impervious fraction of 38% (class urbn) and the grassland parameterization to account for vegetation influence in urban areas. Dead tree areas were represented by the class barren or sparsely vegetated (bsvg) with a slight increase of the fraction of the growing season when leaf area begins to decline (hu_lai_decl from 0.35 to 0.5) to better represent the vegetation period. The generic agriculture class was modelled as winter wheat (wwht) and water bodies were represented by default as a wetland (wetw). Reasonable plant growth was ensured by assessing the development of the leaf area index for all LULC classes. Streams were delineated based on the DEM and a stream map (LGLN 2022) using a threshold of 0.2 km².

Eight weather stations were available in and nearby the catchment area, provided by the German Weather Service (DWD) and the regional water supplier Harzwasserwerke. Precipitation data, daily minimum and maximum temperatures were available at the eight stations, humidity at five stations, wind speed and solar radiation at three stations. Missing values in the weather data were filled using a regression approach and the weather station that showed the highest correlation (Wagner et al. 2012). Remaining gaps were filled using the station with the second highest correlation. Due to the small number of stations with recorded wind speed, an additional station (Braunlage) was considered for gap filling. As solar radiation data at two of the three stations showed large gaps, and the Brocken station had only 5 missing days, the gap-filled global radiation record from the Brocken station was used for the entire catchment. Precipitation data was quality-checked with the help of double mass curves.

To improve the spatial representation precipitation, temperature, humidity and wind speed data were interpolated to a 1 km² grid. Due to the few weather stations and the spatial variability of precipitation in the Harz mountains, interpolation was carried out using a covariate. Usually, a suitable covariate for precipitation is elevation. However, the use of this covariate still resulted in an underestimation of measured streamflow. Therefore, the mean spatial distribution of precipitation (CHELSA data, Karger et al. 2017) was used as a covariate. The precipitation data were interpolated using a regression inverse distance weighting approach at all days at which precipitation showed a significant relationship with the covariate on a weekly basis (Wagner et al. 2012). At the other days, the covariate was not used and an inverse distance weighting approach was used for interpolation. Temperature and humidity were also spatially interpolated in this way using elevation as covariate. As the three stations with wind speed measurements show no significant correlation with altitude, an inverse distance weighting approach was used to interpolate the wind speed. After interpolation, daily values of precipitation, minimum and maximum temperature, relative humidity and wind speed from 1990 to 2023 were available as a model input with a spatial resolution of 1 km.

https://doi.org/10.5194/egusphere-2025-3091
Preprint. Discussion started: 9 September 2025

The SWAT model has been proven to be capable of depicting dynamic LULC change impacts (Nepal et al. 2023, Wagner et al. 2019, 2023). Here we use the land use update tool SWAT-LUT (Morisasi et al. 2019) to apply annual updates to the LULC distribution in the SWAT+ model.

To account for the influence of groundwater, a second groundwater layer was implemented (Pfannerstill et al. 2014, Wagner et al. 2022). The first layer was parameterized for fast groundwater response and the second layer for slow groundwater response. Mostly standard values were used and only three parameters were included in calibration (rchg_dp, alpha_bf, alpha_bf2, Table 1).

Table 1: Calibration parameters and the upper and lower boundaries used for calibration of the SWAT+ model. The last column shows the final calibrated values and adjustments for the absval and abschg change types, respectively.

Parameter	Description	min	max	change	final value/ adjustment
cn2	Curve number condition II	+10	+25	abschg*	+24.8
surlag	Surface runoff lag coefficient	0.1	0.3	absval**	0.235
esco	Soil evaporation compensation coefficient	0.05	0.95	absval	0.051
bd	Bulk density (mg/m³)	+10	+30	pctchg***	+28.9
awc	Available water capacity of the soil layer (mm H_2O/mm soil)	-0.01	+0.08	abschg	-0.009
cn3_swf	Soil water factor for curve number condition III	-20	+20	pctchg	-13.3
perco	Percolation coefficient	0.7	0.98	absval	0.960
rchg_dp	Aquifer percolation coefficient fast to slow aquifer	0.25	0.5	absval	0.478
alpha_bf	Baseflow recession constant fast aquifer	0.5	1	absval	0.695
alpha_bf2	Baseflow recession constant slow aquifer	0.0003	0.005	absval	0.002
snomelt_tmp	Snow melt temperature (°C)	-3	1	absval	-0.840

*abschg adds an absolute value to the initial parameter value; ** absval replaces the initial parameter value with an absolute value, ***pctchg increases or decreases of the initial parameter value by the given percentage of the value

https://doi.org/10.5194/egusphere-2025-3091
Preprint. Discussion started: 9 September 2025

The model was calibrated using Latin Hypercube Sampling to derive 5400 parameter sets for common calibration parameters and ranges given in Table 1. The model with the highest average Kling-Gupta Efficiency for all gauges was selected. The period with dynamic LULC changes from 2018 to 2023 was used for model calibration, assuming that parameters calibrated for dynamically changing LULC conditions, will also be valid for a constant LULC. The period from 2011 to 2017 is used for model validation and the year 2010 as model spin-up time.

2.4 Hydrologic impact assessment

To assess the impacts of continuous LULC changes (tree mortality) on the water resources, two model runs were conducted: i) a model run with the baseline LULC of 2018 and ii) a model run with continuously updated LULC maps (2.2). Both models were run for the same period from 2010 to 2023. Changes in the water balance components (mainly evapotranspiration, water yield, surface runoff, percolation) were assessed by comparing the outputs from the two model runs. In addition, we scale the (uncalibrated) output of the model for sediment yield to the maximum changes, to derive an indicator of changed erosion risk. Spatial as well as temporal changes are analyzed.

3. Results

3.1 Evaluation of LULC classifications

Test data from 2020, 2021 and 2018 were used to assess the accuracy of the satellite-derived LULC classification (Table 2). The accuracy assessment based on test data from 2020 and 2021 indicated an acceptable overall accuracy of 88% for the LULC classification. Among the seven classes, cropland achieved the highest F1-score (97%), whereas dead tree had the lowest F1-score (69%) and precision (56%). The remaining classes achieved satisfactory accuracy, with F1-scores exceeding 0.70.

Table 2: Assessment metrics for the LULC classification based on test data from 2020, 2021, and 2018.

	Based on test data from 2020 and 2021			Based on test data from 2018		
Class	Precision	Recall	F1-score	Precision	Recall	F1-score
Grassland	0.76	0.65	0.70	0.84	0.41	0.56
Cropland	0.96	0.97	0.97	0.98	0.89	0.93
Built-up	0.67	0.88	0.76	0.40	0.92	0.56
Water	0.93	0.91	0.92	0.98	0.81	0.88
Coniferous tree	0.87	0.71	0.78	0.76	0.93	0.83
Deciduous tree	0.84	0.97	0.90	0.88	0.97	0.92
Dead tree	0.56	0.88	0.69	0.69	0.54	0.61
Overall accuracy		0.88			0.86	

https://doi.org/10.5194/egusphere-2025-3091
Preprint. Discussion started: 9 September 2025

Additionally, the accuracy assessment, conducted by comparing the 2018 predicted LULC map with the ELC-10 ground truth data for 2018, indicated an overall accuracy of 86% (Table 2). As shown in Table 2, similar to the metrics from 2020 and 2021, a higher F1-score was observed for cropland. For the dead tree class, precision, recall, and F1-score were 69%, 54%, and 61%, respectively, indicating an improvement in precision but a decrease in recall and F1-score compared to the 2020 and 2021 results.

For the 2023 evaluation, accuracy metrics were calculated with a specific focus on dead tree classification due to limited ground truth availability for other land cover classes. Manual annotation efforts were concentrated exclusively on dead tree samples, resulting in a similar performance as the 2018 data (Table 2) with precision, recall, and F1-scores of 72%, 50%, and 59%, respectively.

3.2 Land use and land cover change analysis

In 2018, the LULC map was predominantly comprised of coniferous trees, accounting for approximately 92.8% (16.79 km²), 91.6% (5.57 km²), and 85.4% (27.02 km²) of the Radau, Gose, and Oker catchments, respectively (Table 3). The small remaining areas of all catchments consisted of other classes, including deciduous trees, grasslands and built-up areas. Figure 3 illustrates the changed and unchanged areas, in which the changed areas depict the LULC from the 2023 classification for all three catchments. As shown in Figure 3, the major changes between 2018 and 2023 are changes to the classes of dead trees and grassland.

Additionally, a transition matrix and net changes in LULC classes across all catchments from 2018 to 2023 were calculated and are presented in Table 3 and Figure 4. The diagonal values in the transition matrix represent LULC classes that remained unchanged between 2018 and 2023. The transition analysis revealed that between 2018 and 2023, 52.1% (9.42 km²), 78.7% (4.78 km²), and 69.4% (21.95 km²) of the LULC remained unchanged in the catchments of the Radau, Gose, and Oker, respectively, while 47.9% (8.67 km²), 21.3% (1.22 km²), and 30.6% (9.68 km²) experienced changes. As Table 3 and Figure 4 show, the Radau catchment exhibited the strongest LULC changes. Particularly grassland/regrown areas expanded from 1.33% (0.24 km²) in 2018 to 31.2% (5.65 km²) in 2023. Additionally, dead tree areas in the Radau catchment increased from 0.05% (0.01 km²) in 2018 to 14.42% (2.61 km²) in 2023. Coniferous tree areas decreased significantly from 92.81% (16.79 km²) in 2018 to 46.82% (8.47 km²) in 2023, primarily due to their conversion into dead tree and grassland/regrown areas during this period. No significant changes were observed in the deciduous tree class (4.25% to 5.58%) between 2018 and 2023. The Gose catchment also experienced an increase in grassland and deciduous trees at the cost of coniferous forest (Table 3 and Figure 4). The area covered by grassland increased by 13.08% (0.84 km²), whereas deciduous trees increased from 7.91% (0.48 km²) to 12.66% (0.77 km²). No dead trees were recorded in 2018, but by 2023, they covered 0.49% (0.03 km²). Coniferous forest cover declined over this period, from 91.76% (5.57 km²) to 72.65% (4.41 km²). In the Oker catchment (Table 3 and Figure 4) grassland increased significantly by 16.03 percentage points (from 0.88 km² to 5.95 km²) while deciduous tree cover increased by 2.65 percentage points (from 2.96 km² to 3.80 km²). The area of dead trees also

https://doi.org/10.5194/egusphere-2025-3091
Preprint. Discussion started: 9 September 2025

showed a net increase of 6.03%. Meanwhile, coniferous tree cover declined by 25.45 percentage points (from 27.02 km² to 18.97 km²). No significant change in built-up areas or water bodies were detected in the three catchments.

A visual analysis of the initial occurrence of dead tree areas showed a spatio-temporal pattern of deforestation between 2018 and 2023 (Figure 5). Dead tree areas were first observed near the Brocken in the Harz mountains, and these areas expanded steadily over the years from the southeast towards the central and western parts of the study area.

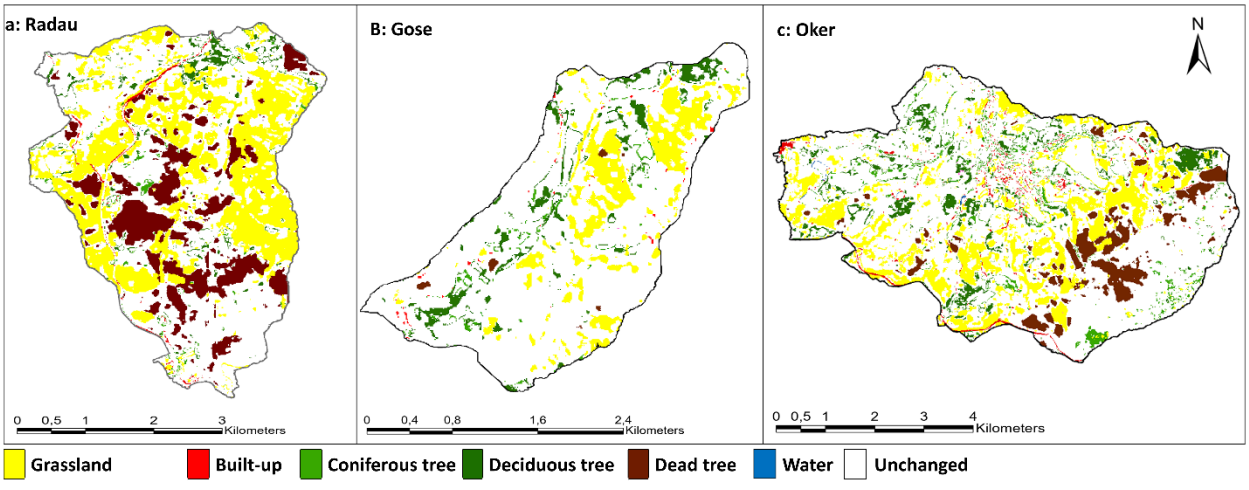

Figure 3: Land use and land cover change in the catchments (a: Radau, b: Gose, c: Oker): Areas that have been changed between 2018 and 2023 are depicted with the LULC of 2023. Unchanged areas are shown in white.

https://doi.org/10.5194/egusphere-2025-3091
Preprint. Discussion started: 9 September 2025

Table 3: Transition matrix of LULC classes for the catchments (Radau, Gose and Oker) from 2018 to 2023 (in km^2).

	Radau	LULC in 2023					Total 2018
		Grassland	**Built-up**	**Coniferous tree**	**Deciduous tree**	**Dead tree**	
LULC 2018	Grassland	0.23	0	0.01	0	0	0.24
	Built-up	0.02	0.25	0.02	0	0	0.28
	Coniferous tree	5.37	0.10	8.32	0.39	2.61	16.79
	Deciduous tree	0.03	0	0.12	0.62	0	0.77
	Dead tree	0	0	0	0	0	0
	Total 2023	5.65	0.35	8.47	1.01	2.61	18.08

	Gose	**LULC in 2023**					**Total 2018**
		Grassland	**Built-up**	**Coniferous tree**	**Deciduous tree**	**Dead tree**	
LULC 2018	Grassland	0	0	0	0	0	0
	Built-up	0	0.01	0.01	0	0	0.02
	Coniferous tree	0.84	0.02	4.34	0.34	0.03	5.57
	Deciduous tree	0	0	0.05	0.43	0	0.48
	Total 2023	0.84	0.03	4.41	0.77	0.03	6.07

	Oker	**LULC in 2023**						**Total 2018**
		Grassland	**Built-up**	**Water**	**Coniferous tree**	**Deciduous tree**	**Dead tree**	
LULC 2018	Grassland	0.83	0	0	0.04	0.01	0	0.88
	Built-up	0.01	0.51	0	0.10	0.01	0	0.62
	Water	0	0	0.15	0.01	0	0	0.15
	Coniferous tree	5.04	0.33	0.01	18.20	1.53	1.91	27.02
	Deciduous tree	0.06	0	0	0.64	2.26	0	2.96
	Total 2023	5.95	0.84	0.16	18.97	3.80	1.91	31.63

https://doi.org/10.5194/egusphere-2025-3091
Preprint. Discussion started: 9 September 2025

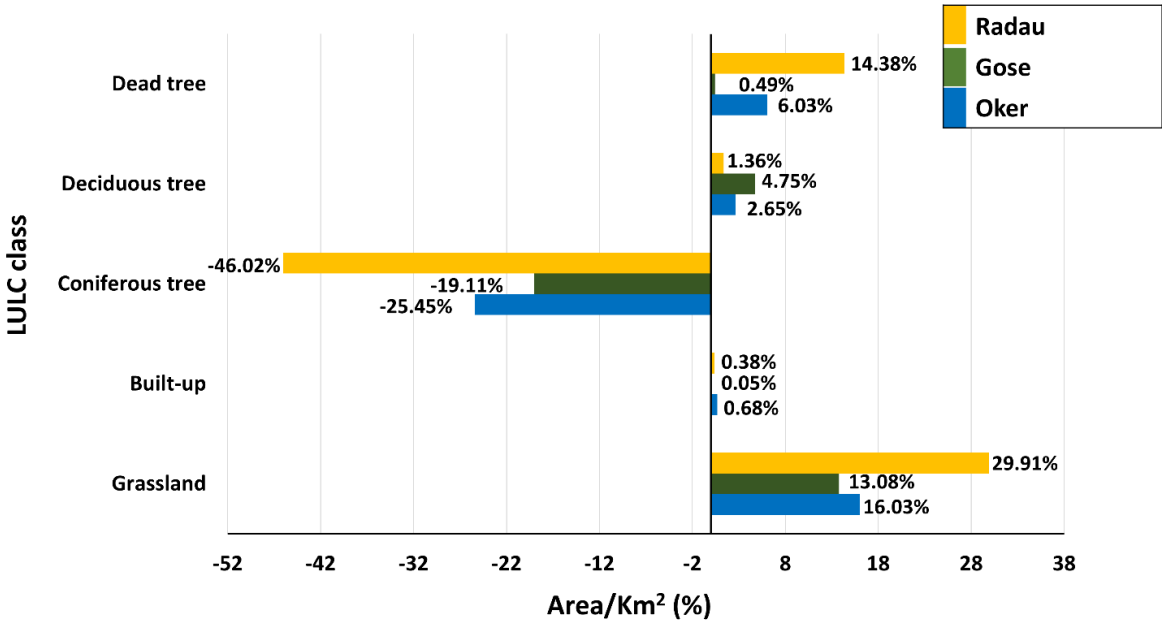

Figure 4: Percentage of net changes in LULC classes across all catchments from 2018 to 2023.

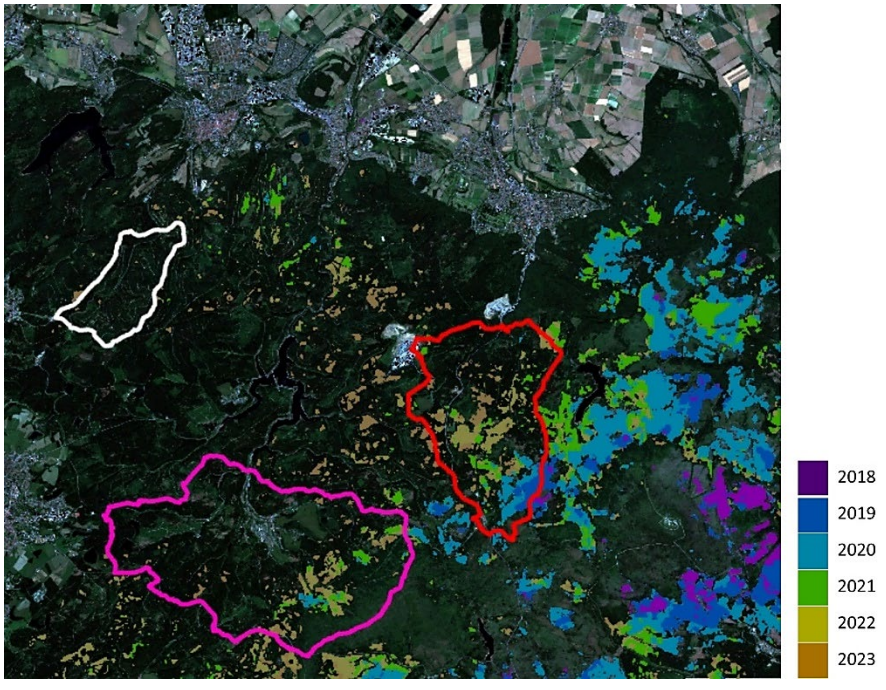

Figure 5: Initial occurrence map of dead trees areas from 2018 to 2023, overlaid on a true color composition Sentinel-2 image with catchment outlines: red for the Radau catchment, white for the Gose catchment, and pink for the Oker catchment.

https://doi.org/10.5194/egusphere-2025-3091
Preprint. Discussion started: 9 September 2025

3.3 Hydrologic model evaluation

Overall model performance is reasonable judged by KGE values during the calibration period (0.75-0.82). The validation period shows a decrease in performance at the gauges Sennhütte (by -0.19 in KGE) and Bad Harzburg (by -0.08 in KGE) and an increase at gauge Altenau (+0.04). Observed streamflow is underestimated during the calibration period by -6.2% to -10.7% (PBIAS, Table 3). During the validation period the underestimation is very low at the gauges Sennhütte and Altenau (PBIAS between -1.0% and -1.8%), but an overestimation by +18.0% can be observed at gauge Bad Harzburg. This gauge generally shows a lower performance as the other two gauges – particularly with regard to the representation of streamflow dynamics as indicated by the NSE (Table 3). Similarly, the hydrographs show that the same events are often replicated with different accuracies at the three gauges, e.g. the event at the beginning of 2020 is well represented at gauge Sennhütte but strongly overestimated at gauge Bad Harzburg, whereas the event at the end of 2023 is best represented at gauge Bad Harzburg (Figure 6). Both, hydrograph and flow duration curves show an underestimation of peak flows (Figure 6 and 7). At gauge Bad Harzburg mid flows are overestimated and low flows are underestimated. At the other two gauges mid and low flow segments of the flow duration curves are well represented by the model (Figure 7).

Table 3: Comparison of goodness-of-fit indicators: Nash-Sutcliffe efficiency (NSE), percentage bias (PBIAS), Kling-Gupta efficiency (KGE) and ratio of the root mean square error (RMSE) between simulated and observed values to the standard deviation of the observations (RSR).

	calibration			validation		
	Sennhütte (Gose)	Altenau (Oker)	Bad Harzburg (Radau)	Sennhütte (Gose)	Altenau (Oker)	Bad Harzburg (Radau)
NSE	0.69	0.68	0.56	0.57	0.66	0.51
PBIAS (%)	-6.6	-10.7	-6.2	-1.8	-1.0	18.0
KGE	0.82	0.75	0.78	0.63	0.79	0.70
RSR	0.55	0.57	0.66	0.65	0.58	0.70

https://doi.org/10.5194/egusphere-2025-3091
Preprint. Discussion started: 9 September 2025

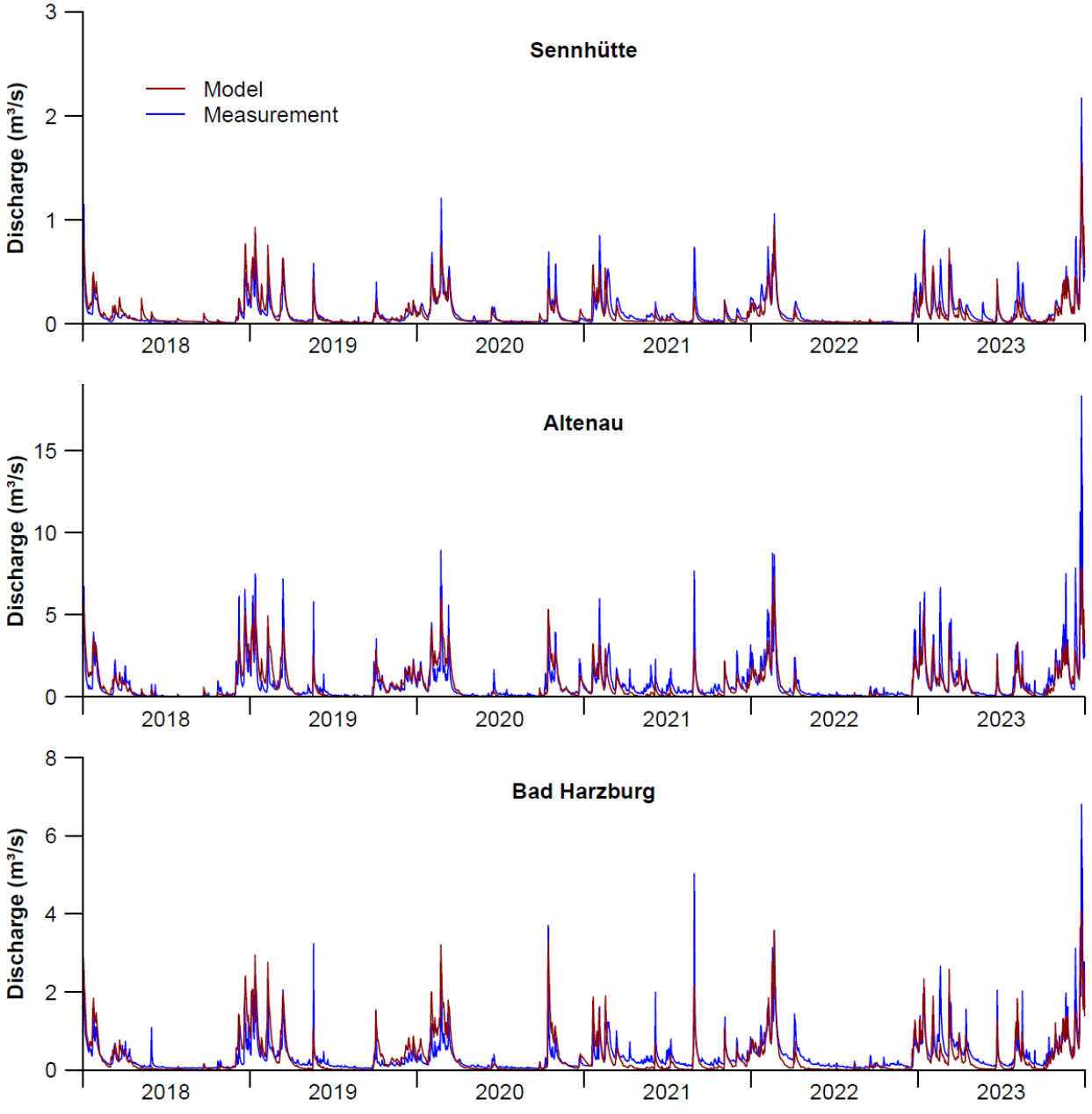

Figure 6: Comparison of modeled and measured hydrographs at all gauges for the calibration period (1 January 2018 – 31 December 2023).

https://doi.org/10.5194/egusphere-2025-3091
Preprint. Discussion started: 9 September 2025

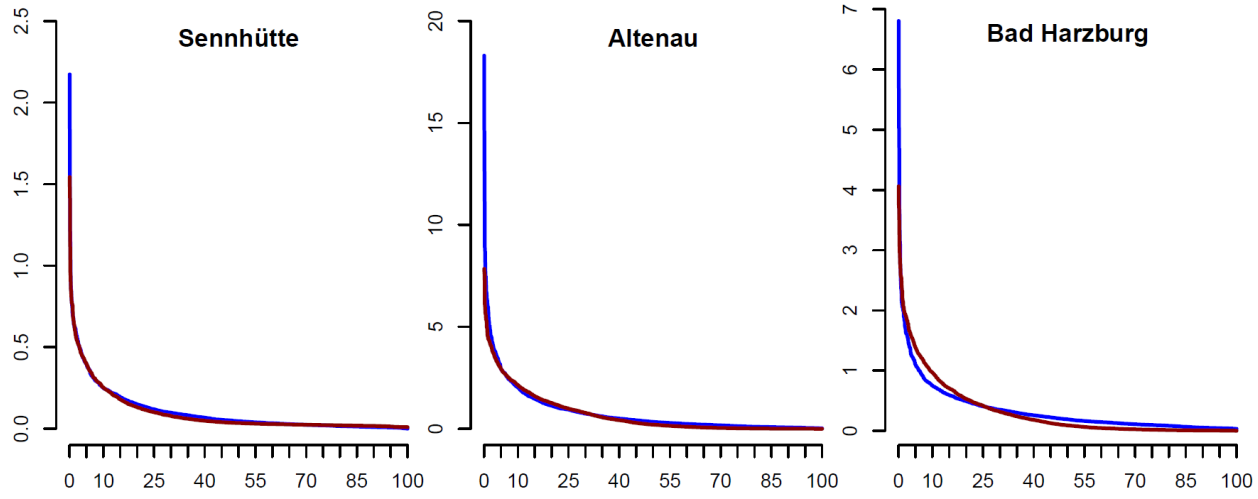

Figure 7: Comparison of measured and modeled flow duration curves at all gauges for the calibration period (1 January 2018 – 31 December 2023).

3.3 Temporal assessment of land use and land cover change impacts

The assessment of LULC change impacts shows a dynamic response of the water balance components, starting with the first updated LULC map in 2019 and increasing towards 2023. In response to tree mortality, model results show a general increase in water yield and a decrease in evapotranspiration. These changes can be attributed to the loss of vegetation, resulting in decreased transpiration and consequently more water yield. Decreases in evapotranspiration can particularly be observed during the vegetation period. Moreover, the increase in water yield can be attributed to an increase in surface runoff as the monthly differences between the averaged changes in all three catchments in water yield and surface runoff are smaller than 0.2 mm. Major increases in water yield occur in months with more precipitation (Figure 8, r=0.57 for averaged changes in all catchments between 2019 and 2023). This effect is stronger between 2021 and 2023 (r=0.76), when tree mortality affects more areas and the impacts are more pronounced. Against the general trend water yield showed major decreases in March 2020 and in March 2022 by up to 5% and 33%, respectively (strongest change in the Radau catchment, Figure 8). This effect can be traced back to the dominance of recession phases in these months. While LULC changes led to increased peak flows, water yield is lower during the recession phase (Figure 9). March 2022 had the lowest precipitation in the investigation period (14 mm average for all catchments) and soil water storage increased by up to 21% (Radau catchment). Moreover, evapotranspiration increased in June 2022 in all catchments (strongest change by +15% in the Gose catchment) and in June 2023 in the Gose (+4%) and Oker (+1%) catchment. The increased evapotranspiration demand is supplied from soil water storage as the increase in soil water storage is smaller as compared to the previous month (May) whereas changes in percolation were small in these months (Figure 8).

https://doi.org/10.5194/egusphere-2025-3091
Preprint. Discussion started: 9 September 2025

While all three catchments show an increase in water yield and a decrease in evapotranspiration, the strength of the response varies. The Radau catchment shows the strongest and the Gose catchment the lowest response. This aligns very well with the magnitude of LULC changes (e.g. percentage of dead tree areas) in these catchment (Figure 4). Moreover, the eastern catchments (Oker and Radau) that have experienced tree mortality earlier (Figure 5) show an earlier response than the Gose catchment in the west, where the first major changes in the water balance components can be observed in the year 2021 (Figure 8). The strength of changes affects the strength of impacts: Assessing changes in the final year (2023) the model shows that the loss of coniferous forest by 46% led to an increase in water yield by 11.3% and a decrease in ET by -7.4% in the Radau catchment. In the Gose and the Oker catchment a loss of coniferous forest by 19% and 25%, led to a water yield increase by 2.8% and 3.1% and a decrease in ET by -2.2% and -3.4%, respectively. Hence, the response in water yield is 4.1 (Radau) to 8.1 (Oker) times smaller and the response in ET is 6.2 (Radau) to 8.6 (Gose) times smaller than the main LULC change in coniferous forest.

https://doi.org/10.5194/egusphere-2025-3091
Preprint. Discussion started: 9 September 2025

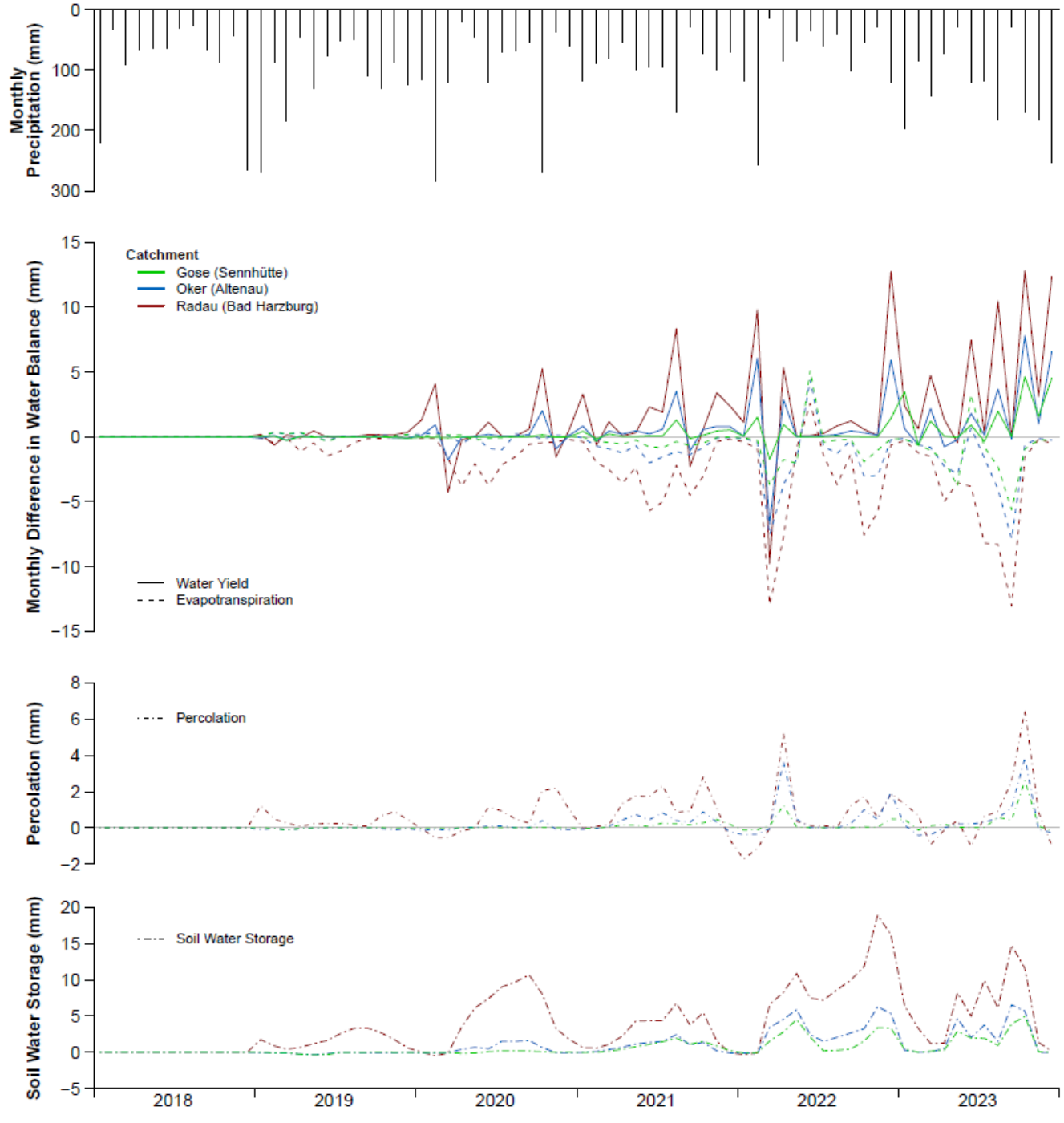

Figure 8: Temporal impacts of dynamic LULC changes on evapotranspiration, water yield, percolation and soil water storage in the three headwater catchments.

https://doi.org/10.5194/egusphere-2025-3091
Preprint. Discussion started: 9 September 2025

340

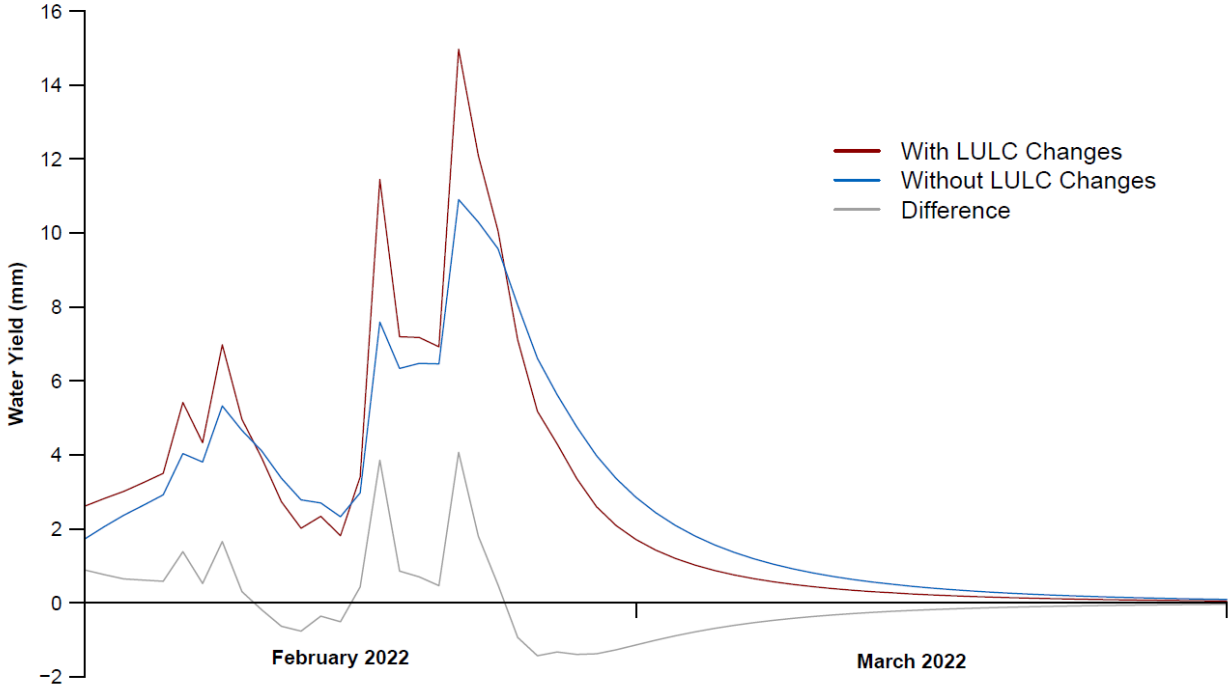

Figure 9: Impact of LULC changes on the hydrograph in the Radau catchment.

345 **3.4 Spatial assessment of land use and land cover change impacts**

The spatial assessment shows how tree mortality affects the water balance components. Areas that were changed from forest to dead trees or grassland are clearly visible, showing a decrease in evapotranspiration and an increase in surface runoff and percolation. Figure 10 underscores the continuous increase of impacts, as in 2019 only one major area of dead trees in the Radau catchment was present and major impacts were associated with this area. In the following years, the percentage of
350 affected areas increased continuously. It has to be noted that the percentage increase shown in Figure 10 shows stronger changes in years, in which low values were present in the baseline, e.g., in relatively dry years like 2021. Moreover, the response also depends on the other characteristics of the HRUs, i.e. the soil and slope class. Particularly, peat soils present in the catchment of the Radau showed a stronger response, as surface runoff was comparatively low with unchanged conditions. The patterns of erosion risk underline increased erosion risk on dead tree areas. These correspond to areas with
355 changes in surface runoff, as changes in sediment yield and surface runoff are correlated (r=0.71 between absolute changes in both variables).

https://doi.org/10.5194/egusphere-2025-3091
Preprint. Discussion started: 9 September 2025

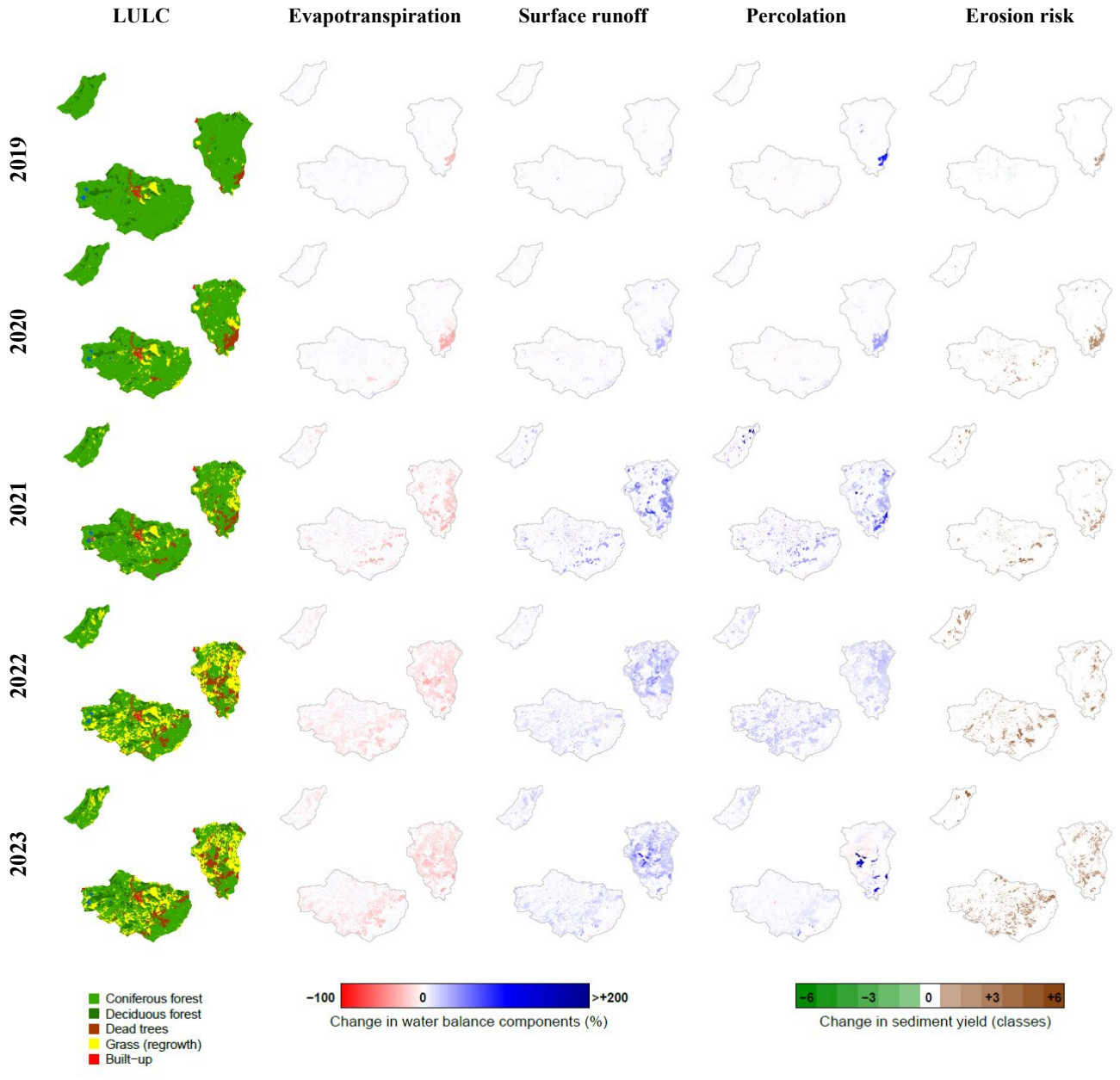

Figure 10: Spatio-temporal impacts of dynamic LULC changes on evapotranspiration, surface runoff, percolation and erosion risk in the three headwater catchments.

https://doi.org/10.5194/egusphere-2025-3091
Preprint. Discussion started: 9 September 2025

4. Discussion

4.1 Land use and land cover change

LULC classifications from 2018 to 2023 were generated by combining a U-Net architecture with multi-temporal, multi-sensor satellite data. This approach integrated spectral bands and vegetation indices from Sentinel-2, as well as VV and VH polarizations from Sentinel-1. The accuracy assessment based on the test data from 2020 and 2021 demonstrated good model performance, with an overall accuracy of 88%. Additionally, the results indicated that cropland achieved higher accuracy metrics than the other classes, likely due to the higher number of training samples available (40% of the total training samples). Conversely, the dead tree class demonstrated a lower accuracy, which can be attributed to the limited number of samples for this class (1% of total training samples). Furthermore, the acceptable accuracy score (overall accuracy of 86%) achieved by comparing the ELC-10 map with the 2018 predicted LULC map underscores the reliability of this method. The lower F1-scores for all LULC classes in 2018, except for coniferous and deciduous trees, compared with those in 2020 and 2021, may be attributed to differences in the reliability of the ground truth data. For training and testing, we used ESA maps from 2020 and 2021, which had overall accuracies of 75% and 77%, respectively (ESA WorldCover 2020, 2021), whereas the ELC-10 dataset had an overall accuracy of 90% (Venter & Sydenham, 2021). Notably, we selected ESA maps (2020/2021) over ELC-10 (2018) for model training to exploit their larger training sample sizes.

For the dead tree class, the F1-score in 2023 declined compared to that in 2020 and 2021 (59% vs. 69%), likely due to forest loss and regrowth on formerly dead tree areas. Similarly, the F1-score in 2018 was lower than that in 2020 and 2021 (61% vs. 69%), despite fewer dead trees being present in 2018. This decline is related to a low recall value for the dead tree class, suggesting an underestimation of dead trees due to a higher number of false negatives. It has to be acknowledged that the shift from a healthy state to a dead state occurs gradually. Consequently, areas in the intermediate stages of defoliation were not accounted for, potentially leading to misclassification and reduced accuracy of the dead tree class. This may also contribute to confusion between coniferous trees and dead trees (see confusion matrix in Appendix, Figure A1). Furthermore, the management strategy in the Harz mountains, where dead trees are removed to prevent bark-beetle infestations and regrowth of grass and shrubs occurs (Thonfeld et al., 2022), contributes to minor confusion between dead trees and grassland (Figure A1). These confusions have intensified in 2022–2023 as tree mortality increased. It is also worth noting that the precision for dead trees improved by 13% in 2018 and 16% in 2023 compared to that in 2020 and 2021, likely because of the majority voting approach used to generate annual LULC prediction maps.

The analysis also indicated a similar trend in the net LULC changes across all catchments from 2018 to 2023 (Figures 3 and 4), with dead tree and grassland areas expanding primarily at the cost of coniferous forests. The decline in coniferous trees can be linked to tree mortality caused by bark beetle infestations and prolonged drought, particularly from 2018 to 2022 (Knapp et al., 2024). Drought both directly and indirectly contributes to an increase in dead trees and a decline in coniferous forest cover by weakening the natural defenses of trees against infestation (Rohde et al., 2021). Furthermore, the increase in

https://doi.org/10.5194/egusphere-2025-3091
Preprint. Discussion started: 9 September 2025

grassland can be attributed to the fact that regrowth of dead tree areas is classified as grassland. Therefore, both, the dead tree and the grassland areas shall be used as a proxy of total LULC changes due to deforestation.

As shown in Figures 3 and 4, the Radau catchment experienced the most significant changes, with the highest conversion of coniferous trees to grassland and dead tree areas compared to the other two catchments. Given the found spatio-temporal development with an expansion of tree mortality from the south-east to the (north-)west, it can be expected that the other catchments may expect further and more severe changes in the future, particularly if drought conditions apply.

4.2 Hydrologic impacts

We attribute the differences in measured and modeled discharge to (i) the precipitation input as well as to (ii) trade-offs associated with the derivation of one set of parameters for all gauges. Although a better spatial representation of precipitation (i) was achieved by applying an interpolation scheme, the low density of precipitation stations in this heterogeneous mountain region still limits the possibilities to improve the spatial representation of the precipitation input. Particularly small catchments like the Gose catchment upstream of gauge Sennhütte are affected by non-representative precipitation patterns. The closest precipitation gauge for this catchment is located at the Grane reservoir at a lower elevation and at the northern edge of the Harz mountains. For example, a local event occurred on 22 May 2023 with 23 mm recorded in Grane, whereas only about 2 mm rainfall were recorded in the upstream (Schulenberg and Brocken). The stronger reaction to this local event shown in the measurements (increase by 0.157 m^3/s in mean daily discharge as compared to the previous day) indicates that the measured data from the downstream was probably more representative for the catchment than the measured data from the upstream or the used interpolated data that only let to an increase by 0.0024 m^3 mean daily discharge in the model. With regard to model parameters (ii), trade-offs of multi-gauge calibration are clearly shown when analyzing the optimum range of the surface runoff lag coefficient (surlag) judged by the NSE that is at the lower end of the applied parameter range for the gauge Bad Harzburg and at the upper end for the gauge Altenau. Consequently, an optimization for the individual gauges with regard to KGE (i.e. a single gauge calibration) would yield a better representation of dynamics for Bad Harzburg (NSE: 0.61, KGE: 0.79, PBIAS: -7.7%), whereas the performance increase at gauge Sennhütte and Altenau is negligible (improvement of NSE $\leq$ 0.01 and KGE $\leq$ 0.02) during the calibration period.

The LULC change observed in the Harz mountains is probably the most extreme LULC change in Germany in recent years and it is of particular importance to depict such extreme changes in models as this is a prerequisite for accurate impact assessment and management of impacts. The continuous increase of the hydrological impacts of LULC change underline the capability of SWAT+ to depict LULC change in space and time (Nepal et al. 2023, Wagner et al. 2019, 2023) and the successful implementation of SWAT-LUT for SWAT+ (Moriasi et al. 2019).

The found increase of water yield and decrease of evapotranspiration as a consequence of tree mortality are generally reasonable and in agreement with the literature (Adams et al. 2012, McGinn et al. 2021, Zhang et al. 2017). In a synthesis of disturbance effects in coniferous forests, Goeking and Tarboton (2020) found that evapotranspiration sometimes increased

https://doi.org/10.5194/egusphere-2025-3091
Preprint. Discussion started: 9 September 2025

after forest loss due to higher subcanopy radiation and increased transpiration of postdisturbance growth. Such effects were considered in two ways: 1) dead tree areas were modeled as barren or sparsely vegetated, and 2) areas with vegetation were classified as grassland / regrown areas. However, we found that -although these effects were accounted for-, a decrease in evapotranspiration dominated on the catchment scale. In fact, model results show that transpiration from plants and evaporation from interception in the canopy decreased whereas soil evaporation increased.

Moreover, the results shed light on possible consequences. Due to forest loss and decreased evapotranspiration, the catchments react faster. In particular, the extremes are exacerbated as peak flows are increased and low flows are decreased (Figure 9). This increases the probability and frequency of flood events in the downstream – where a major flood event had already led to significant damage in 2017, i.e. before the major LULC changes. In addition, increased erosion risk on dead tree areas is plausible given very low erosions rates in undisturbed forests. These pose an additional risk during flood events and likely contribute to faster sedimentation of reservoirs, like the Oker reservoir downstream of gauge Altenau.

5. Conclusion

Driven by drought conditions the Harz mountains experienced tree mortality and exceptional changes in LULC between 2018 and 2023. The strength of these LULC changes has strong impacts on hydrology. Consequently, these changes need to be considered in hydrologic models.

LULC changes were detected using a synergistic combination of Sentinel-2 optical imagery and Sentinel-1 radar data, processed through a U-Net deep learning architecture. The model achieved robust performance, with both visual interpretation and quantitative accuracy metrics, confirming the reliability of our results. The analysis revealed widespread coniferous forest decline, particularly in the Radau catchment where coverage dropped from 93% to 47%, accompanied by substantial increases in dead tree areas and grassland expansion. While the growing season-focused model showed reasonable accuracy (overall accuracy = 86-88%) future improvements incorporating longer sequence data could enhance detection robustness. Furthermore, since some misclassification might be attributed to the uncertainty of ESA maps (with an overall accuracy of 75–77%) and manual dead tree annotation errors, future work could focus on label refinement.

The SWAT+ model proofed capable of representing these changes and their spatio-temporal impacts on hydrology. In general, a decrease in evapotranspiration and an increase in surface runoff, percolation, and erosion risk were found. The strength of impacts increased over time with the increasing loss of coniferous forests. Moreover, the spatial impact assessment showed that impacts can be traced back to dead tree areas. As a consequence of the observed changes, the catchments respond faster leading to increased flood probability and frequency in downstream areas. In particular, hydrological extremes are exacerbated due to an increase in peak flows and a decrease in low flows. Afforestation with climate-resilient trees could improve both, the resilience to droughts and floods in regions with drought-induced tree mortality like the Harz mountains.

https://doi.org/10.5194/egusphere-2025-3091
Preprint. Discussion started: 9 September 2025

Code availability: SWAT+ is an open source model available from https://swat.tamu.edu/.

Data availability: Model input data is available from the cited data providers. Model output data is available from the authors upon reasonable request.

Competing interests: The authors declare that they have no conflict of interest. PW is a member of the editorial board of HESS.

Author contributions:

Conceptualization: PW; Methodology: PW, SF, and PA; Investigation, formal analysis, data curation, visualization, and writing (original draft preparation): PW and SF; Funding acquisition: PW and NF; Writing (review and editing): all authors. All authors have read and agreed to the published version of the manuscript.

Acknowledgements

We acknowledge funding by the German Federal Ministry of Education and Research (BMBF) through the funding measure "Hydrological extreme events (WaX)". Model simulations were performed on the high performance computing clusters at Kiel University.

References

Adams, H. D., Luce, C. H., Breshears, D. D., Allen, C. D., Weiler, M., Hale, V. C., Smith, A., and Huxman, T. E.: Ecohydrological consequences of drought-and infestation-triggered tree die-off: insights and hypotheses, Ecohydrology, 5(2), 145-159, 2012.

Arnold, J.G., Srinivasan, R., Muttiah, R.S., and Williams, J.R.: Large area hydrologic modeling and assessment - Part 1: Model development, J. Am. Water Resour. Assoc. 34, 73-89, 1998.

Auerswald, K., Geist, J., Quinton, J. N., and Fiener, P.: HESS Opinions: Floods and droughts – are land use, soil management, and landscape hydrology more significant drivers than increasing CO2?, Hydrol. Earth Syst. Sci., 29, 2185–2200, https://doi.org/10.5194/hess-29-2185-2025, 2025. BGR (Bundesanstalt für Geowissenschaften und Rohstoffe): Bodenübersichtskarte 1:200.000 (BÜK200), 2022.

Bevacqua, E., Rakovec, O., Schumacher, D. L., Kumar, R., Thober, S., Samaniego, L., Seneviratne, S. I., and Zscheischler, J.: Direct and lagged climate change effects intensified the 2022 European drought, Nature Geoscience, 1-8, 2024.

Bieger, K., Arnold, J.G., Rathjens, H., White, M.J., Bosch, D.D., Allen, P.M., Volk, M., and Srinivasan, R.: Introduction to SWAT+, a Completely Restructured Version of the Soil and Water Assessment Tool, J. Am. Water Resour. Assoc 53(1), 115-130, 2017.

Blickensdörfer, L., Oehmichen, K., Pflugmacher, D., Kleinschmit, B., and Hostert, P.: National tree species mapping using Sentinel-1/2 time series and German National Forest Inventory data. Remote Sensing of Environment, 304, 114069, https://doi.org/10.1016/J.RSE.2024.114069, 2024.

https://doi.org/10.5194/egusphere-2025-3091
Preprint. Discussion started: 9 September 2025

ESA WorldCover: https://worldcover2020.esa.int/, 2020.

ESA WorldCover: https://worldcover2021.esa.int/, 2021.

Fernández-Manso, A., Fernández-Manso, O., and Quintano, C.: SENTINEL-2A red-edge spectral indices suitability for discriminating burn severity. International Journal of Applied Earth Observation and Geoinformation, 50, 170–175, https://doi.org/10.1016/J.JAG.2016.03.005, 2016.

Gitelson, A. A., Kaufman, Y. J., and Merzlyak, M. N.: Use of a green channel in remote sensing of global vegetation from EOS-MODIS, Remote Sensing of Environment, 58(3), 289–298, https://doi.org/10.1016/S0034-4257(96)00072-7, 1996.

Goeking, S.A. and Tarboton, D.G.: Forests and water yield: A synthesis of disturbance effects on streamflow and snowpack in western coniferous forests. J. For., 118 (2) (2020), 172-192, 10.1093/jofore/fvz069, 2020.

Hou, Y., Wei, X., Zhang, M., Creed, I. F., McNulty, S. G., and Ferraz, S.F.: A global synthesis of hydrological sensitivities to deforestation and forestation, Forest Ecology and Management, 529, 120718, 2023.

Huete, A.R.: A soil-adjusted vegetation index (SAVI). Remote Sensing of Environment, 25(3), 295–309, https://doi.org/10.1016/0034-4257(88)90106-X, 1988.

Karger, D. N., Conrad, O., Böhner, J., Kawohl, T., Kreft, H., Soria-Auza, R. W., Zimmermann, N.E., Linder, H.P., and Kessler, M.: Climatologies at high resolution for the earth's land surface areas, Scientific data, 4, 170122, https://doi.org/10.1038/sdata.2017.122, 2017.

Knapp, N., Wellbrock, N., Bielefeldt, J., Dühnelt, P., Hentschel, R., and Bolte, A.: From single trees to country-wide maps: Modeling mortality rates in Germany based on the Crown Condition Survey, Forest Ecology and Management, 568, https://doi.org/10.1016/j.foreco.2024.122081, 2024.

Kong, X., Ghaffar, S., Determann, M., Friese, K., Jomaa, S., Mi, C., Shatwell, T., Rinke, K., and Rode, M.: Reservoir water quality deterioration due to deforestation emphasizes the indirect effects of global change, Water Research 221, 118721, https://doi.org/10.1016/j.watres.2022.118721, 2022.

LBEG (Landesamt für Bergbau Energie und Geologie): Bodenkarte von Niedersachsen 1:50 000, 2024.

LGLN (Landesamtes für Geoinformation und Landesvermessung Niedersachsen): Auszug aus den Geodaten des Landesamtes für Geoinformation und Landesvermessung Niedersachsen, 2022.

McGinn, A. J., Wagner, P. D., Htike, H., Kyu, K. K., and Fohrer, N.: Twenty years of change: Land and water resources in the Chindwin catchment, Myanmar between 1999 and 2019, Science of the Total Environment, 798, 148766, 2021.

Moriasi, D. N., Pai, N., Steiner, J. L., Gowda, P. H., Winchell, M., Rathjens, H., Starks, P. J., and Verser, J. A.: SWAT-LUT: A desktop graphical user interface for updating land use in SWAT, JAWRA Journal of the American Water Resources Association, 55(5), 1102-1115, 2019.

Nepal, D., Parajuli, P.B., Ouyang, Y., To, S.D.F., and Wijewardane, N.: Assessing hydrological and water quality responses to dynamic landuse change at watershed scale in Mississippi, Journal of Hydrology, 625, Part A, 129983, https://doi.org/10.1016/j.jhydrol.2023.129983, 2023.

https://doi.org/10.5194/egusphere-2025-3091
Preprint. Discussion started: 9 September 2025

Peñuelas, J., and Sardans, J.: Global Change and Forest Disturbances in the Mediterranean Basin: Breakthroughs, Knowledge Gaps, and Recommendations. Forests, 12, 603, 2021.

Pfannerstill, M., Guse, B., and Fohrer, N.: A multi-storage groundwater concept for the SWAT model to emphasize nonlinear groundwater dynamics in lowland catchments, Hydrological Processes, 28(22), 5599–5612, 2014.

Rakovec, O., Samaniego, L., Hari, V., Markonis, Y., Moravec, V., Thober, S., Hanel, M., and Kumar, R.: The 2018–2020 multi-year drought sets a new benchmark in Europe. Earth's Future, 10, e2021EF002394. https://doi.org/10.1029/2021EF002394, 2022.

Rohde, M. Langer, G., Hurling, R., and Plasil, P.: Waldschutzsituation 2020 in Nordwestdeutschland, AFZ-Wald 76, 42–46, 2021.

Ronneberger, O., Fischer, P., and Brox, T.: U-net: Convolutional networks for biomedical image segmentation. Lecture Notes in Computer Science (Including Subseries Lecture Notes in Artificial Intelligence and Lecture Notes in Bioinformatics), 9351, 234–241, https://doi.org/10.1007/978-3-319-24574-4_28, 2015.

Rouse, J. W., Haas, R. H., Schell, J. A., and Deering, D. W.: Type II Report for the Period, 1973.

Sutmöller, J., and Meesenburg, H.: Einfluss von forstlicher Bestandesentwicklung und Klimawandel auf Wasserhaushaltskomponenten im Einzugsgebiet der Langen Bramke im Harz, Hydrologie & Wasserbewirtschaftung, 62, 184-198, 2018.

Thonfeld, F., Gessner, U., Holzwarth, S., Kriese, J., da Ponte, E., Huth, J., and Kuenzer, C.: A First Assessment of Canopy Cover Loss in Germany's Forests after the 2018–2020 Drought Years, Remote Sensing, 14(3), https://doi.org/10.3390/rs14030562, 2022.

Venter, Z. S., and Sydenham, M. A. K.: Continental-scale land cover mapping at 10 m resolution over europe (Elc10), Remote Sensing, 13(12), https://doi.org/10.3390/rs13122301, 2021.

Wagner, P. D., Bieger, K., Arnold, J. G., and Fohrer, N.: Representation of hydrological processes in a rural lowland catchment in Northern Germany using SWAT and SWAT+, Hydrological Processes, 36(5), e14589, 2022.

Wagner, P. D., Bhallamudi, S. M., Narasimhan, B., Kumar, S., Fohrer, N., and Fiener, P.: Comparing the effects of dynamic versus static representations of land use change in hydrologic impact assessments, Environmental Modelling & Software, 122, 103987, 2019.

Wagner, P.D., Fiener, P., Wilken, F., Kumar, S., and Schneider, K.: Comparison and evaluation of spatial interpolation schemes for daily rainfall in data scarce regions, Journal of Hydrology, 464, 388-400, 2012.

Wagner, P. D., Kumar, S., and Fohrer, N.: Integrated modeling of global change impacts on land and water resources, Science of The Total Environment, 892, 164673, 2023.

Xu, H.: Modification of normalised difference water index (NDWI) to enhance open water features in remotely sensed imagery, International Journal of Remote Sensing, 27(14), 3025–3033, https://doi.org/10.1080/01431160600589179, 2006.

https://doi.org/10.5194/egusphere-2025-3091
Preprint. Discussion started: 9 September 2025

Xu, H.: A new index for delineating built-up land features in satellite imagery, International Journal of Remote Sensing, 29(14), 4269–4276, https://doi.org/10.1080/01431160802039957, 2008.

Zha, Y., Gao, J., and Ni, S.: Use of normalized difference built-up index in automatically mapping urban areas from TM imagery, International Journal of Remote Sensing, 24(3), 583–594, https://doi.org/10.1080/01431160304987, 2003.

Zhang, M., Liu, N., Harper, R., Li, Q., Liu, K., Wei, X., Ning, D., Hou, Y. and Liu, S.: A global review on hydrological responses to forest change across multiple spatial scales: Importance of scale, climate, forest type and hydrological regime, Journal of Hydrology, 546, 44-59, 2017.

Appendix

Table A1: Computed indices and their formulae.

	Vegetation indices	Formula	Reference
NDVI	Normalized Difference Vegetation Index	(NIR-Red)/(NIR+Red)	(Rouse et al., 1973)
GNDVI	Green Normalized Difference Index	(NIR-Green)/(NIR+Green)	(Gitelson et al., 1996)
NDVI_red edge	Red Edge Normalized Difference Vegetation Index	(NIR-Red_edge)/(NIR+Red_edge)	(Fernández-Manso et al., 2016)
SAVI	Soil-Adjusted Vegetation Index	((NIR-Red)/(NIR+Red+L)) × (1+L)	(Huete, 1988)
MNDWI	Modified Normalized Difference Water Index	(Green-SWIR)/(Green+SWIR)	(Xu, 2006)
NDBI	Normalized Difference Built-up Index	(SWIR-NIR)/(SWIR+NIR)	(Zha et al., 2003)
IBI	Index-based Built-up Index	(NDBI-(SAVI+MNDWI)/2)/ (NDBI+(SAVI+MNDWI)/2)	(Xu, 2008)

Note: NIR: near-infrared, SWIR: short wave infrared, and L = 0.428

https://doi.org/10.5194/egusphere-2025-3091
Preprint. Discussion started: 9 September 2025

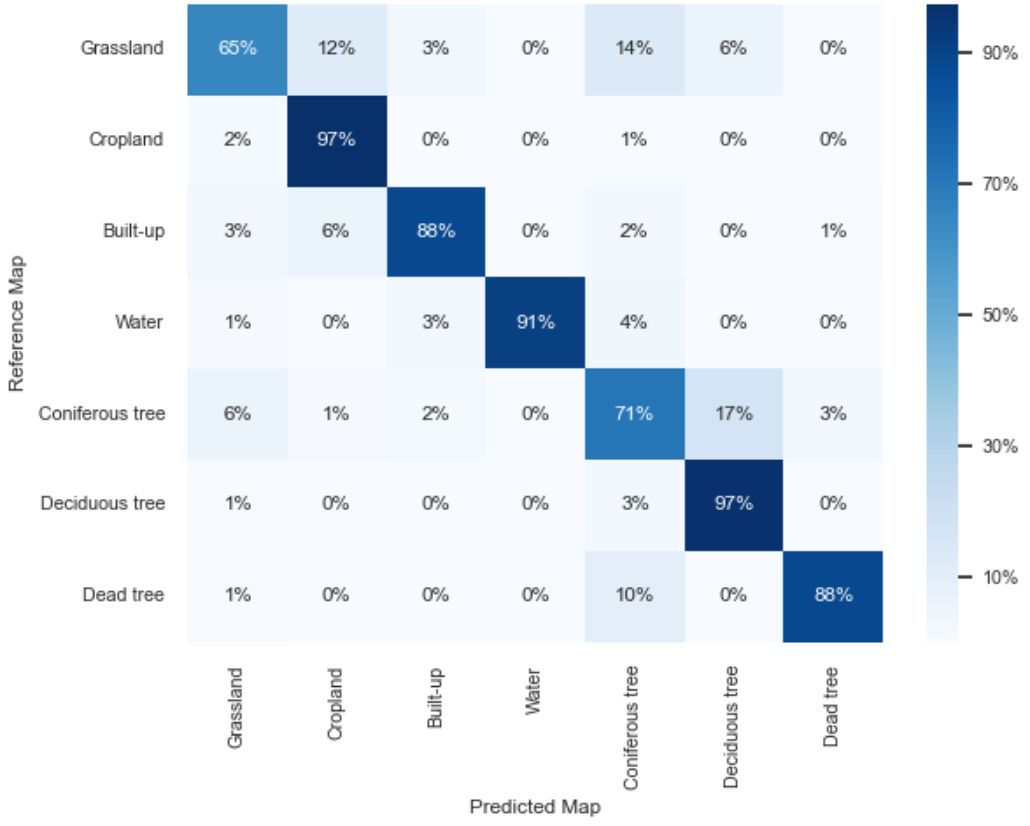

570

Figure A1: Confusion matrix based on test data from 2020 and 2021.